frontiers in Marine Science

ORIGINAL RESEARCH
published: 05 November 2020
doi: 10.3389/fmars.2020.594725

Inter-annual Variability of the Carbonate System in the Hypoxic Upper Pearl River Estuary in Winter

Xianghui Guo[1,2,3], Xue Song[1,2], Ying Gao[1,2], Yaohua Luo[1,2], Yi Xu[1], Tao Huang[1] and Lifang Wang[1,2]*

[1] State Key Laboratory of Marine Environmental Science, Xiamen University, Xiamen, China, [2] College of Ocean and Earth Sciences, Xiamen University, Xiamen, China, [3] Fujian Provincial Key Laboratory for Coastal Ecology and Environmental Studies, Xiamen University, Xiamen, China

Hypoxia has become a universal environmental and ecological problem in recent decades. The Pearl River estuary (PRE), the largest estuary in Southern China, is hypoxic year-round in the upper estuary. This study reports the inter-annual variation between 2005 and 2019 in the carbonate system of the hypoxic upper PRE in winter. In January 2005, both dissolved inorganic carbon (DIC) and total alkalinity (TA) concentrations were >3000 μmol kg^{-1} at the upstream-most station and decreased sharply downstream. However, DIC and TA were lower, with concentrations of 2300 and 1950 μmol kg^{-1}, respectively, at the upstream-most in January 2019. At salinities >15, both DIC and TA were conservative and reached steady values at the downstream seawater end-member. The upstream-most station was taken as an example to quantify the influences of biogeochemical processes on DIC and TA, including CO_2 degassing, organic carbon oxidation, pelagic nitrification, $CaCO_3$ dissolution and benthic release. Among the biogeochemical process, a decrease in $CaCO_3$ dissolution (from 734.4 μmol kg^{-1} in 2005 to 168.9 μmol kg^{-1} in 2019) was the major factor driving the decreases of DIC and TA in 2019. In the context of global change, inter-annual variability in biogeochemical process should receive more attention.

Keywords: Pearl River estuary, carbonate system, inter-annual variability, biogeochemical processes, hypoxic

OPEN ACCESS

Edited by:
Zhan Hu,
School of Marine Sciences (CAS), China

Reviewed by:
Meilin WU,
South China Sea Institute of Oceanology (CAS), China
Sun Cuici,
South China Sea Institute of Oceanology (CAS), China

****Correspondence:***
Xianghui Guo
xhguo@xmu.edu.cn

Specialty section:
This article was submitted to Coastal Ocean Processes, a section of the journal Frontiers in Marine Science

Received: *14 August 2020*
Accepted: *12 October 2020*
Published: *05 November 2020*

Citation:
Guo X, Song X, Gao Y, Luo Y, Xu Y, Huang T and Wang L (2020) Inter-annual Variability of the Carbonate System in the Hypoxic Upper Pearl River Estuary in Winter. Front. Mar. Sci. 7:594725. doi: 10.3389/fmars.2020.594725

HIGHLIGHTS

- A significant inter-annual variation in DIC and TA in the hypoxic upper Pearl River estuary was observed between 2005 and 2019.
- Processes influencing DIC and TA were quantified in the hypoxic upper Pearl River estuary.

INTRODUCTION

Hypoxia in estuaries and coasts is a global environmental and ecological problem (Caballero-Alfonso et al., 2015; Fennel and Testa, 2019). Well-known hypoxic zones include the northern Gulf of Mexico (Rabalais and Turner, 2006), the Baltic Sea (Conley et al., 2011; Bendtsen and Hansen, 2013; Carstensen et al., 2014), Chesapeake Bay (Testa and Kemp, 2012; Li et al., 2016), and the East

China Sea off the Changjiang estuary (Li et al., 2002), as well as others. The Pearl River estuary (PRE) is the largest estuary in southern China, and is surrounded by several rapidly developing cities such as Guangzhou, Dongguan, Shenzhen, and others. Hypoxia in the PRE occurs mainly in two zones; one is the year-round hypoxic zone in the upper estuary from Guangzhou to Humen (Zhai et al., 2014), and the other is the seasonal hypoxic zone in summer at the estuary mouth and in waters near Hong Kong (Qian et al., 2018; Wang et al., 2018; Cui et al., 2019). In the hypoxic upper estuary, highly over-saturated CO_2 was observed all year round, with CO_2 partial pressures (pCO_2) up to >7000 μatm and dissolved inorganic carbon (DIC) concentration up to >3000 μmol kg^{-1} in winter (Xu et al., 2005; Dai et al., 2006, 2008; Guo et al., 2008; Zhai et al., 2014).

Viewing the entire PRE, Guo et al. (2008) reported the seasonal variability of carbonate parameters in the main channel of the estuary based on field observations from 2000 to 2005; Liang et al. (2020) simulated the spatial distributions of carbonate parameters in the summer and winter of 2006. In the hypoxic upper PRE, Guo et al. (2008) found that both DIC and total alkalinity (TA) showed large seasonal variations, with much higher values in winter (>3000 μmol kg^{-1}) than in summer (<1700 μmol kg^{-1}). They suggest that seasonal changes in the location of freshwater end-member, biogeochemical processes and hydrologic conditions are the major causes of the variability (Guo et al., 2008). More recently, field observations since 2010 have shown lower DIC and TA values (<2500 μmol kg^{-1}) in winter in the upper PRE (Dai et al., unpublished data). However, DIC and TA of the river waters were much lower than 2000 μmol kg^{-1} (Guo et al., unpublished data). This indicates that the very high DIC and TA concentrations previously found in the upper PRE in winters from 2000 to 2005 might be due to strong local additions from biogeochemical processes.

This study aims to: (1) confirm that DIC and TA in the upper PRE decreased after 2005, and (2) determine the key processes dominating the inter-annual variability in these parameters. In order to solve these two questions, we closely compare data collected from January 2005 and January 2019 in the estuary. The 2005 data were previously published (Guo et al., 2008), and the 2019 data were collected during a cruise at nearly the same locations in the upper PRE as the 2005 data. During the cruise, in addition to measuring carbonate system parameters, dissolved oxygen (DO) and nutrient measurements, and oxygen consumption and nitrification incubations were conducted using the same methods as in January 2005.

MATERIALS AND METHODS

Study Area

The Pearl River is the 2nd largest river in China and the 13th largest river in the world in terms of freshwater discharge, with an annual freshwater discharge of 3.3×10^{11} m^3 $year^{-1}$ (Zhao, 1990; Dai et al., 2014). The Pearl River has three major tributaries: the West River, the North River and the East River, and many local rivers and reticulated channels in the delta (**Figure 1**). The West River originates from the Yunnan–Guizhou Plateau and flows though Yunnan Province, Guizhou Province, the Guangxi Zhuang Autonomous Region and Guangdong Province. The North River and the East River originate from Jiangxi Province and flow through Guangdong Province. The three major tributaries contribute ∼95% of the freshwater discharge of the Pearl River system (Zhao, 1990). The drainage basins of the West River and North River have an abundance of carbonate minerals, while the drainage basin of the East River is rich in silicate minerals. Therefore, the bicarbonate and calcium concentrations in the West and North Rivers are higher than in the East River (Chen and He, 1999). The drainage basin of the Pearl River system is located in the south Asia tropical and subtropical areas, and ∼80% of the freshwater discharge occurs during the wet season from April to October, driven by the Asian monsoon (Zhao, 1990; Dai et al., 2014). The highest discharges of the three main tributaries occur from June to July, and lowest discharges are in winter (December–February, **Figure 2**).

All runoff from the Pearl River system discharges into the northern South China Sea (NSCS) via eight major outlets (from east to west: the Humen, Jiaomen, Hongqimen, Hengmen, Modaomen, Jitimen, Hutiaomen, and Yamen outlets) and through three sub-estuaries: the Lingdingyang, Modaomen, and Huangmaohai (**Figure 1**). Lingdingyang is traditionally called the PRE, which collects the freshwater from the eastern four outlets, including the East River and branches of the North and West Rivers.

The lower Pearl River drainage basin has several rapidly developing cities, such as Guangzhou, Dongguan, and others. Rapid economic and population growth have caused serious environmental problems, such as water pollution and hypoxia. In the early 2000s, whole water column hypoxia and very high ammonia concentrations (>800 μmol kg^{-1} in winter and >300 μmol kg^{-1} in summer) were observed in the upper estuary from Guangzhou to Humen (Dai et al., 2008). Strong aerobic respiration and nitrification induced very high pCO_2 and CO_2 degassing rates (Dai et al., 2006, 2008; Guo et al., 2008). Due to dilution by seawater and relatively weaker biogeochemical processes downstream, nutrient concentrations and pCO_2 decreased sharply downstream of the Humen Outlet, i.e., in the Lingdingyang (Dai et al., 2006; Guo et al., 2009).

Over the past few decades, sewage discharge and treatment rates have both significantly increased. For example, in the city Guangzhou, urban domestic sewage discharge increased from 7.4 billion tons $year^{-1}$ in 1995 to 14.3 billion tons $year^{-1}$ in 2015 (**Figure 3A**). At the same time, the sewage treatment rate also increased, from <10% in 1995 to 48% in 2005, and then to >85% after 2010 (**Figure 3B**). Subsequently, direct sewage discharge without treatment decreased sharply after 2005 (**Figure 3C**) (Bulletin of Statistics of Guangzhou's Environmental Status).[1] As a result, the water quality of the channels flowing through Guangzhou and Dongguan has improved considerably. During the January 2005 cruise, the water was black, had a noticeably bad smell, and wildlife such as fish and birds were not observed. However, in 2019, we observed greener water, flock of egrets, and the absence of previous odors. Therefore, 2005 is a

[1] http://sthjj.gz.gov.cn/gkmlpt/index

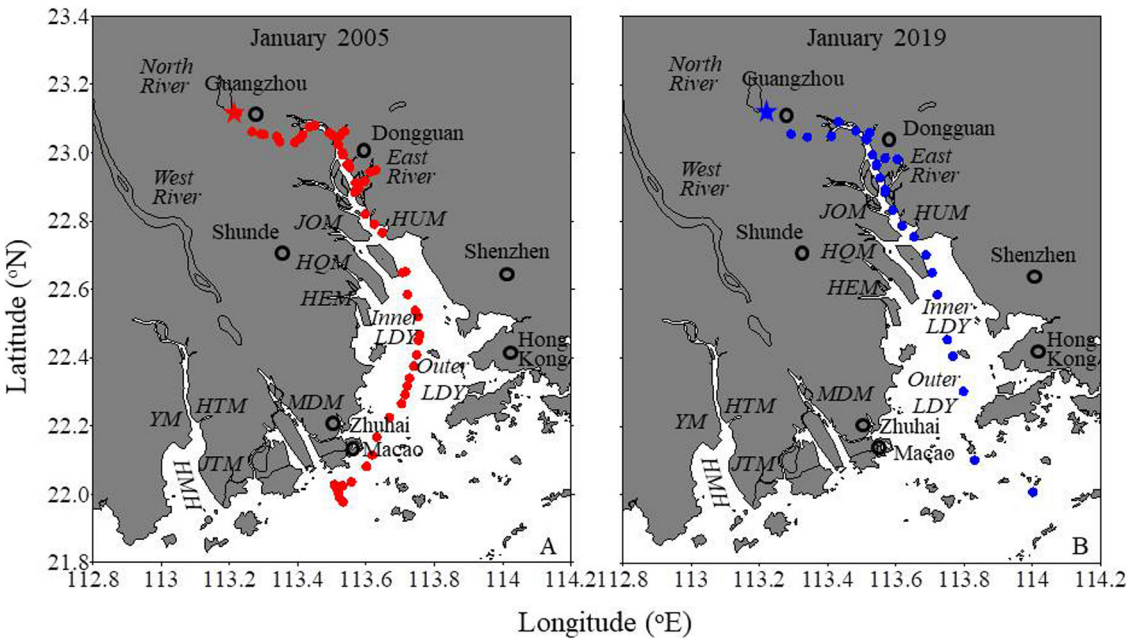

FIGURE 1 | The map of the Pearl River estuary with sampling stations (dots). HUM, JOM, HQM, HEM, MDM, JTM, HTM, and YM are the outlets of Humen, Jiaomen, Hongqimen, Hengmen, Modaomen, Jitimen, Hutiaomen, and Yamen. The black open circles mark the cities. LDY is the Lingdingyang; HMH is the Huangmaohai. The star is the incubation station. Data for the January 2005 cruise are from Guo et al. (2008).

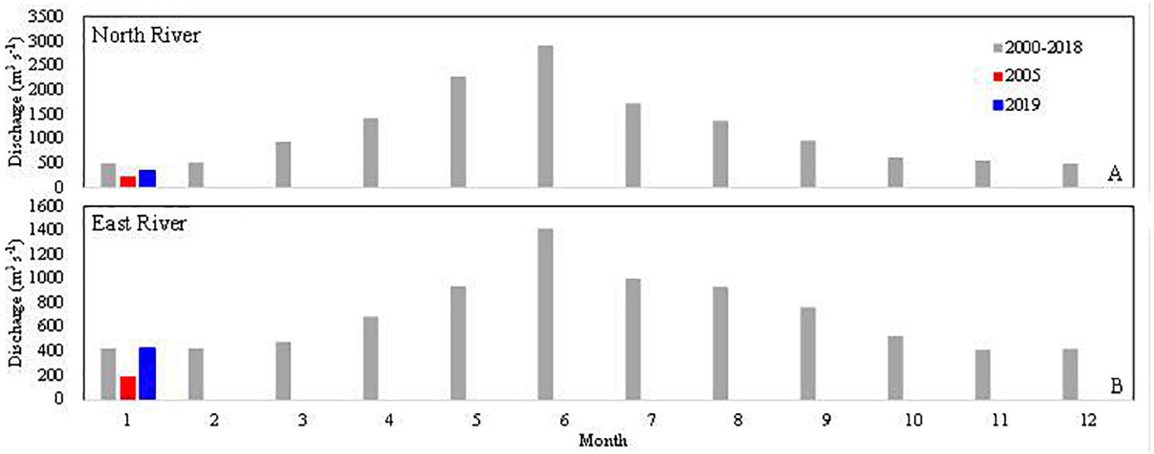

FIGURE 2 | Freshwater discharge downstream of the North River (Shijiao gauge station) and East River (Boluo gauge station). Label of panel **B** is the same with panel **A**. Data are from the Annual Hydrological Report (2000–2018), Hydrology Bureau, Ministry of Water Resources of the China (http://www.pearlwater.gov.cn/).

representative year of the huge impacts of direct sewage discharge and severe pollution, while 2019 is a representative year of water quality restoration.

Sampling and Analysis

Water Sample Collection

Cruises were conducted in the PRE from January 19–23, 2005, and from January 12–18, 2019, onboard the Yue-Dongguan-Yu 00589 and Yue-Zhu-Yu 31008. At each station, depth profiles of salinity and temperature were recorded with a YSI 6600 multi-parameter monitoring system (2005) or an AML BASE.X (sensor exchangeable Instrument) Conductivity-Temperature-Depth/pressure (CTD) sensor package (2019). Water samples were collected with 2 L or 5 L Niskin bottles.

Sub-samples for DO, pH, DIC/TA were taken with Tygon® tubing free of air bubbles, with ample sample overflow in order to minimize any contamination from atmospheric O_2 or CO_2. Samples for DO were sampled with 60 mL BOD (biological oxygen demand) bottles and fixed with Winkler reagents (Carpenter, 1965). Samples for pH were taken into

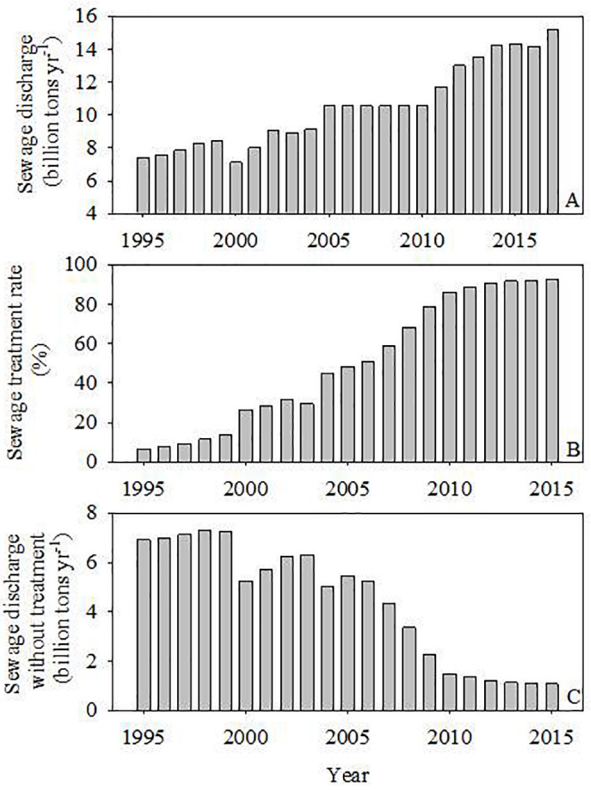

FIGURE 3 | Urban sewage discharges, sewage treatment rate, and sewage discharges without treatment from the city Guangzhou. Each column represents one year. Data were from the Bulletin of Statistics of Guangzhou's Environmental Status (1995–2015), http://sthjj.gz.gov.cn/gkmlpt/content.

120 mL amber glass bottles and poisoned with 100 μL of a saturated $HgCl_2$ solution. During the January 2005 cruise, DIC samples were sampled into 40 mL amber glass vials with 50 μL saturated $HgCl_2$ added; TA samples were sampled into 120 mL high-density Polyethylene (HDPE) bottles with 100 μL saturated $HgCl_2$ added. During the 2019 cruise, samples for DIC and TA measurements were taken into 250 mL borosilicate bottles with grounded stoppers and poisoned with 200 μL of the saturated $HgCl_2$ solution. All DIC and TA samples were stored in the dark at room temperature until analysis. Samples for nutrient and calcium (Ca^{2+}) measurements were filtered with 0.45 μm polyacetate filters. Samples for nitrite (NO_2^-), nitrate and nitrite (N + N), and soluble reactive phosphorus (SRP) were frozen and stored at −20°C until analysis. Samples for ammonium (NH_4^+) and silicate (Si) measurements were stored at −4°C until analysis. Samples for Ca^{2+} measurements were stored in the dark at room temperature.

CO_2 partial pressures of surface water and the atmosphere was measured with an underway system integrating an air-water equilibrator and a Li-Cor 7000 or Picarro G2101-i CO_2 analyzer. Six air-based CO_2 standard gases ranging 200 to 10000 parts per million provided by the National Reference Material Research Center of China were used to calibrate the measurements. Data processing was the same as previously described in Guo et al. (2009). Wind speed was measured with an R.M. Young model 05106 marine wind monitor at ∼10 m above the sea surface. The accuracy of wind speed measurements was ±0.3 m s^{-1}.

In February 18–19 of 2019, surface water samples were collected at gauge stations in the lower North and East Rivers (Shijiao in the North River and Boluo in the East River) to measured DIC, TA, nutrients, and calcium. The samples were taken with a 2 L plexiglass sampler. The sub-sampling, treatment and storage methods are the same as those during the January 2019 cruise.

Rate Incubation Experiments

Bulk oxygen consumption incubations were conducted at the upstream-most station (**Figure 1**) following the method of Dai et al. (2006). Briefly, surface water was pumped into a clean 400 L plastic box. After oxygenation, the water was transferred into two 20 L HDPE cubitainers (Thermo Fisher Scientific) immediately. 10 mL of a saturated $HgCl_2$ solution was added to one of the cubitainers as a control. The incubation was conducted in the dark and the temperature was controlled to match that of the surface water by using running water circulated outside of the cubitainers. Samples were taken every 3–6 h to measure DO. Bulk oxygen consumption rates were estimated from the change in the DO concentration over time.

Incubation experiments for estimating nitrification rates were conducted at the same stations as the bulk oxygen consumption incubations following the method of Dai et al. (2008). Briefly, surface water was sampled with 5 L Niskin bottles. Triplicate samples were filled into 4 L narrow-neck amber glass bottles. Allylthiourea (ATU, final concentration of 100 mg L^{-1}) and $NaClO_3$ (final concentration of 10 mg L^{-1}) were added to the bottles to inhibit the oxidation of NH_4^+ and NO_2^-, respectively. The third bottle was used as a control without reagent addition. Water samples were taken every 4–8 h to measure NO_2^-. NH_4^+ and NO_2^- oxidation rates were estimated from the change in the concentration of NO_2^- over time.

Sample Analysis

Dissolved oxygen samples were measured onboard with the classic Winkler method, and calibrated using a potassium iodate standard solution provided by the Reference Material Center of the Marine Ecology and Environmental Laboratory of the 2nd Institute of Oceanography (Ministry of Natural Resources of the People's Republic of China). The precision of the measurements was better than ±2 μmol kg^{-1}. pH samples were measured onboard within 2 h of sampling with a Corning 350 or Orion 3 Star pH meter and an Orion 8102BN Ross combination electrode calibrated against three NBS buffers (4.01, 7.00, and 10.01 at 25°C, provided by Thermo Fisher Scientific). Samples for pH measurements and buffers were placed in a constant temperature bath at 25 ± 0.01°C for about 1 h before their pH values were measured. Therefore, the measured pH values were at 25°C (pH_{25}) and given on the NBS scale. DIC and TA samples were measured onboard within 1 day of sampling during the 2005 cruise and within 1 week after the 2019 cruise. Analyses of DIC and TA followed the methods previously described by Cai et al. (2004). DIC was measured by collecting and quantifying

the CO_2 released from the sample upon acidification with a non-dispersive infrared detector (Li-Cor 7000) using an Apollo SciTech model AS-C3 DIC Analyzer with a precision of ±2 μmol kg^{-1}. TA was determined by Gran titration with hydrochloric acid using an automated alkalinity titrator (Apollo SciTech model AS-ALK1+) with a precision of better than ±2 μmol kg^{-1}. Both DIC and TA measurements were calibrated with certified reference material (CRM) provided by Dr. A. G. Dickson at the Scripps Institution of Oceanography, to obtain an accuracy of better than ±2 μmol kg^{-1}.

For the January 2019 cruise, Ca^{2+} was measured using the ethylene glycol tetraacetic acid (EGTA) titration method developed by Lebel and Poisson (1976) and modified by Cao and Dai (2011), with a precision of ±0.06%. The measurements were calibrated with artificial seawater based $CaCl_2$ solution. Salinity standard seawater of the International Association for the Physical Sciences of the Oceans (IAPSO) (Batch P158) was adopted as a reference. The measured Ca/salinity ratio of the IAPSO standard seawater was 291.6, which was slightly higher than the reported value of Batch P79 and P86 (290.5 and 290.9) (Olson and Chen, 1982), but slightly lower than the reported values of 292.0 for Batch P78 (Olson and Chen, 1982), 293.0 for Batch P67 (Kanamori and Ikegami, 1980), and 292.3 for Batch P147 (Cao and Dai, 2011). The deviations of the Ca/salinity ratios might be attributed to differences in the ratios of the different batches of the IAPSO standard seawater, and/or the system error among the different laboratories or operators. Nevertheless, our Ca/salinity ratio was very close to the average of the above literature values (291.7). The precision of our measurements (±0.06%) were ±5.8 μmol kg^{-1} for seawater with salinity of 33. For the January 2005 cruise, Ca^{2+} was measured with the ethylenediaminetetraacetic acid (EDTA) titrimetric method (China-EPA, 1987), with a precision of ±0.41%, (±39.5 μmol kg^{-1} for seawater with salinity 33).

Ammonium samples were measured onboard within 3 h of sampling using the indophenol blue method, with a detection limit of 0.1 μmol L^{-1} (Pai et al., 2001). NO_2^- was determined using the pink azo dye method; N + N was determined by copper-cadmium column reduction and the pink azo dye photometric method; SRP was determined with the phosphomolybdenum blue photometric method; silicate samples were determined using the silicomolybdic blue photometric method (Hansen and Koroleff, 1999). NO_2^-, N + N, SRP and silicate samples were all measured with an AA3 Auto-Analyzer (Bran-Lube, GmbH). The detection limits for NO_2^-, N + N, SRP and silicate were 0.04, 0.10, 0.08, and 0.16 μmol L^{-1}, respectively, and the analytical precision was better than 1% for N + N and silicate and 2% for SRP (Han et al., 2012).

Data Processing

The saturation state index (**Ω**) was defined as the product of the concentrations of Ca^{2+} ($[Ca^{2+}]$) and carbonate ($[CO_3^{2-}]$) divided by the apparent solubility product of $CaCO_3$ (K_{sp}^*) (Eq. 1).

$$\Omega = \frac{[Ca^{2+}] \times [CO_3^{2-}]}{K_{sp}^*} \quad (1)$$

$[Ca^{2+}]$ was the measured Ca^{2+} concentration. $[CO_3^{2-}]$ was calculated from DIC and TA with the program CO2SYS (Version 14) (Pierrot et al., 2006). The dissolution constants of carbonic acid are from Millero (2010). The CO_2 solubility coefficient is from Weiss (1974) and the sulfate dissociation constant from Dickson (1990). The PO_4^{3-} and SiO_2 data are the measured cruise data. K_{sp}^* at 1 standard atmosphere pressure was calculated from temperature and salinity according to the formula of Mucci (1983). The pressure correction of the K_{sp}^* of calcite was from Ingle (1975); the pressure correction of the K_{sp}^* of aragonite was from Millero (1979). The calculated **Ω** was 0.02–0.37 higher than the values calculated with CO2SYS, which might suggest the contribution of excess Ca^{2+} produced by the dissolution of $CaCO_3$ in the upper estuary.

DO saturation degree (DO%) was defined as the ratio of the measured DO to the DO at saturation (DO_{sat}) (Eq. 2). DO_{sat} was calculated according to the empirical formula of Benson and Krause (1984).

$$DO\ (\%) = (DO/DO_{sat}) \times 100\% \quad (2)$$

The net CO_2 flux (F_{CO2}) between surface water and the atmosphere (or air-sea CO_2 flux) was calculated using the following formula:

$$F_{CO2} = k \times s \times \Delta pCO_2 \quad (3)$$

$$k = 0.27 \times U_{10}{}^2 \times (Sc/660)^{-0.5} \quad (4)$$

where s is the solubility of CO_2 (Weiss, 1974), ΔpCO_2 is the pCO_2 difference between the surface water and the atmosphere, and k is the CO_2 transfer velocity. k was parameterized using the empirical function of Sweeney et al. (2007). U_{10} is the wind speed at 10 m above sea level (in m s^{-1}). Here, the daily average wind speeds were adopted in the FCO_2 calculations.

RESULTS

Salinity, Temperature and DO Saturation Degree

The freshwater sources of the upper PRE are mainly the North River and the East River. The long-term (2000–2018) monthly average freshwater discharge rates of the North and East Rivers are ∼500 and ∼420 m^3 s^{-1} in winter, equivalent to 25–40% of the freshwater discharge in summer (**Figure 2**). The low freshwater discharge in winter may have resulted in the higher salinities observed in the upper PRE in winter than in summer (salinity was 0 from Guangzhou to Humen in summer, Guo et al., 2008).

During both the January 2005 and 2019 cruises, the salinity of the upstream-most station at Guangzhou was <0.5, and increased downstream (**Figures 4A,B**). Salinity at the Humen Outlet ranged from 10 to 20, and increased to >25 in Outer Lingdingyang and 30–33 at the estuary mouth.

Surface water temperatures ranged from 14.6 to 18.8°C in January 2005, with the higher temperatures found in the low latitude zone (<22°N). In January 2019, temperatures

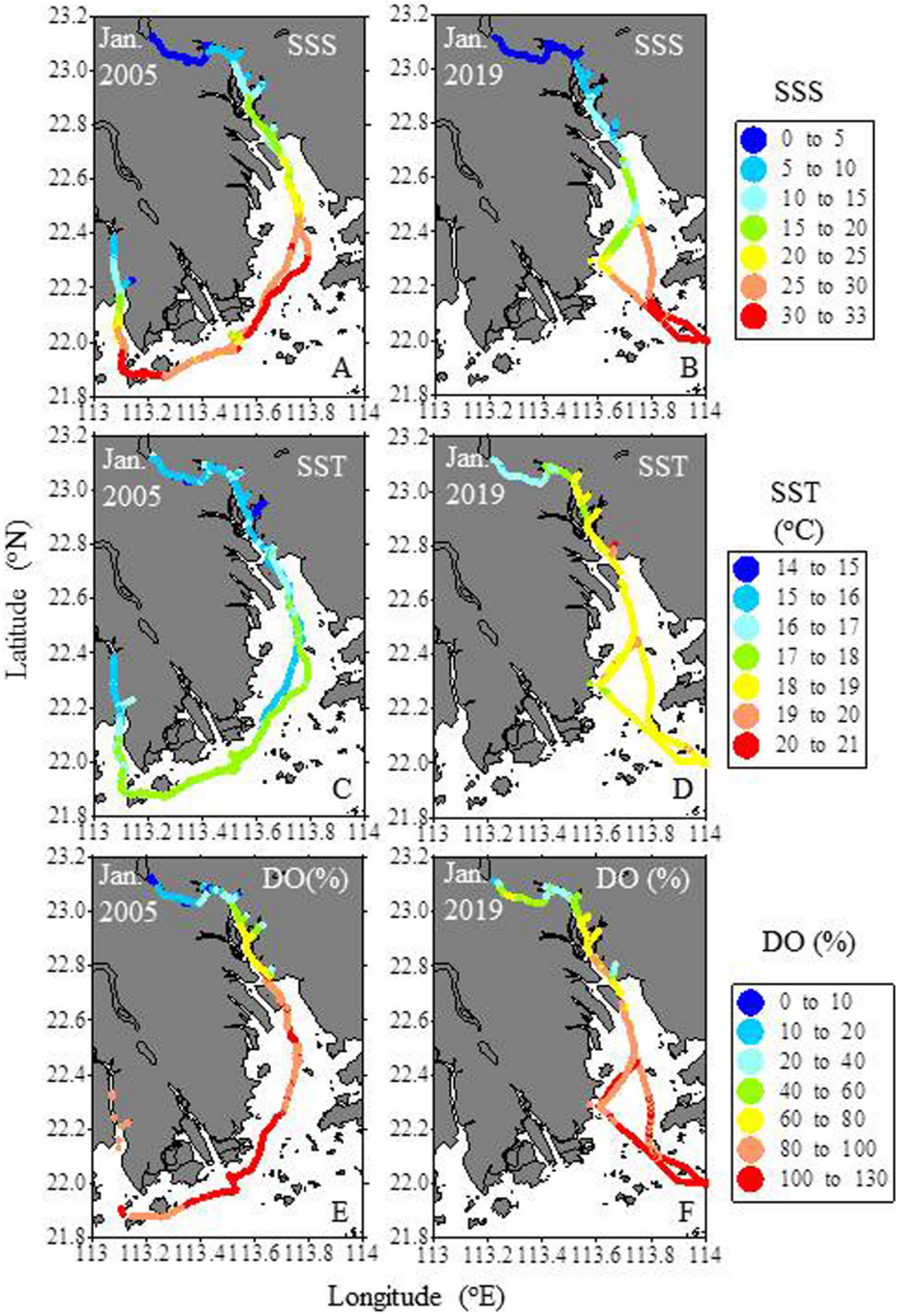

FIGURE 4 | Spatial distributions of salinity (SSS). temperature (SST) and DO saturation degree (DO%) of surface water in the Pearl River estuary in January of 2005 and 2019. The January 2005 data are from Guo et al. (2009).

ranged from 15.9 to 20.5°C, with higher temperatures in the Lingdingyang and outside of the estuary mouth than in the upper estuary (**Figures 4C,D**).

The DO saturation degree in the Guangzhou region ranged from ∼4–31% (12–93 μmol kg^{-1}) in January 2005, and most of this region was hypoxic. Downstream from Guangzhou, the DO saturation degree increased to 60–80% at the Humen Outlet and 80–100% in the Lingdingyang. Outside of the Lingdingyang, DO was slightly oversaturated (**Figure 4E**). In January 2019, DO saturation in the Guangzhou region ranged from 15 to 65% (45–200 μmol kg^{-1}), and hypoxic zones were observed at the two east-west ends of this region. Downstream of Guangzhou, the degree and pattern of DO saturation was similar to that observed in January 2005 (**Figure 4F**). Comparing the data of the two

January cruises reveals that DO was slightly higher in 2019 than in 2005 in the upper estuary (**Figures 4E,F**).

Spatial Distribution of Carbonate System Parameters, DO and Nitrogen-Containing Nutrients

In January 2005, DIC and TA values were as high as ∼3300 and 3100 μmol kg^{-1}, respectively, at the upstream-most station, and decreased sharply downstream. At salinities >15, both DIC and TA showed either a linear decrease or increase with salinity. However, the distributions of DIC and TA in January 2019 were different. At the upstream-most station, DIC and TA concentrations were 2300 and 1950 μmol kg^{-1}, respectively, ∼1000 μmol kg^{-1} lower than those measured at this station in 2005. They both decreased with salinity and reached their minima at salinity of ∼5. At salinities >5, both DIC and TA increased with salinity. Similar to the 2005 survey, at salinities >15, both DIC and TA were conservative (**Figures 5A-1,B-1**). As DIC and TA concentrations in the low salinity zone were much lower in 2019 than in 2005, their concentrations in almost the entire estuarine mixing zone were lower in 2019 than in

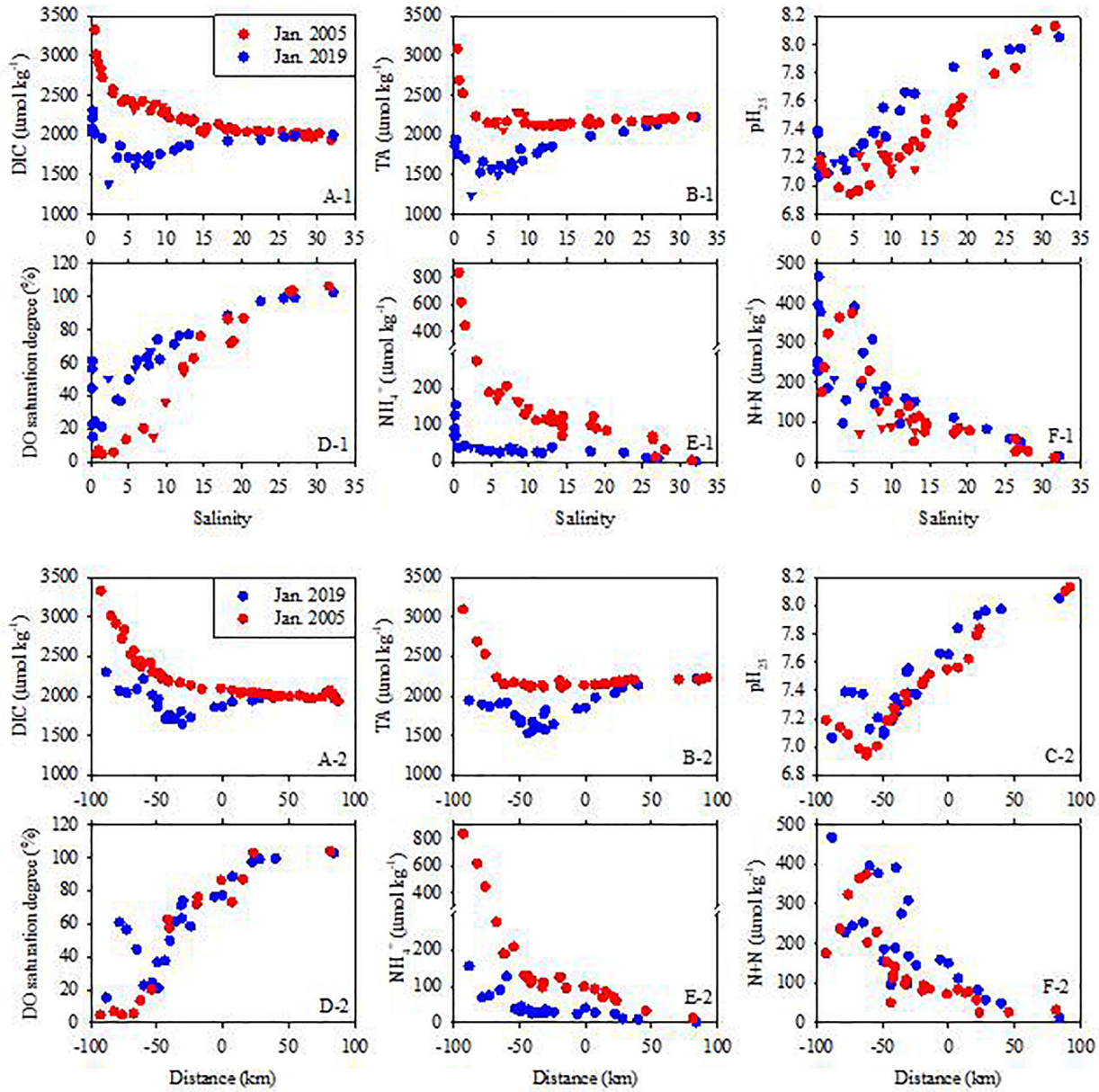

FIGURE 5 | DIC, TA, pH_{25}, DO, ammonium and N + N concentrations in surface water in January of 2005 and 2019. The distance is from Humen Outlet with negative values indicating upstream and positive values downstream locations. The triangles represent the data collected in the lower branches of the East River. For the January 2005 cruise, DIC, TA and pH_{25} data are from Guo et al. (2008), and nutrient data are from Dai et al. (2008). Legends are the same for all panels.

2005 (**Figures 5A-2,B-2**). At salinities >30, TA values in January of 2005 and 2019 were consistent, which indicated the stable characteristics of the seawater compared to the estuarine water (**Figure 5B-1**).

In January 2005, the pH at the upstream-most station was ∼7.2. pH decreased downstream and reached a minimum (6.9) at a salinity of ∼5 (**Figure 5C-1**), which was due mainly to the high rates of nitrification and aerobic respiration (Guo et al., 2008). At salinities >5, pH increased downstream and reached ∼8.11 at a salinity of ∼33 (**Figure 5C-1**). In January 2019, the distribution of pH in the upper estuary was slightly different from that in 2005. Although the pH at the upstream-most station was as low as 7.06, the pH in the middle of the Guangzhou region was as high as ∼7.4 (**Figure 5C-2**). pH decreased again to 7.1 further downstream (60 km upstream Humen Outlet), and then increased with salinity to 8.05 at a salinity of 32.5. Compared with 2005, DO in the Guangzhou region in 2019 was generally higher. However, at the same site downstream of Guangzhou (from the distance of −50 km downstream), the DO saturation degree in 2019 resembled January 2005 (**Figure 5D-2**). The relatively higher pH at stations in the Guangzhou region in January 2019 was accompanied by higher DO concentrations (**Figures 5C-2,D-2**).

In January 2005, NH_4^+ concentrations in the most upper estuary were as high as 800 μmol kg^{-1} and decreased sharply downstream to 3 μmol kg^{-1} at salinities >30 (**Figures 5E-1,E-2**). N + N concentrations increased from 177 μmol kg^{-1} at the upstream-most station to a maximum of 372 μmol kg^{-1} at a salinity of ∼5, and then decreased to 10 μmol kg^{-1} at salinities >30 (**Figures 5F-1,F-2**). The sharp decrease in NH_4^+ concentrations and maximum N + N concentrations in the low salinity zone were due to the presence of strong nitrification (Dai et al., 2008; Guo et al., 2008). In January 2019, the NH_4^+ concentration at the upstream-most station was 150 μmol kg^{-1}, much lower than in 2005. Consequently, NH_4^+ concentrations across the entire estuarine mixing zone were much lower in 2019 than in 2005. However, the N + N concentration at upstream-most stations (up to 463 μmol kg^{-1}) was higher than in 2005 (**Figures 5E-1,E-2,F-1,F-2**). This might be due mainly to the nitrification process during sewage treatment (EPA, 1993). The total concentration of NH_4^+ and N + N at the upstream-most station was also much lower in 2019 than in 2005 (1009.6 vs. 622.7 μmol kg^{-1}), which might be due to the denitrification process during sewage treatment (EPA, 1993).

Distribution of Calcium, and the Saturation State Index of Calcium Carbonate

Calcium concentrations ranged from 1798 to 9410 μmol kg^{-1} in January 2005 and from 989 to 9529 μmol kg^{-1} in January 2019. Although generally the Ca^{2+} concentration increased with salinity, the overall distribution of Ca^{2+} was slightly different between the two winter cruises. In 2005, Ca^{2+} concentrations in the low salinity zone were higher than in 2019. If the conservative mixing line between the North River and seawater was taken as a reference, Ca^{2+} concentrations showed additions in the low salinity zone in January of both 2005 and 2019, and the addition in 2005 was higher than in 2019.

The saturation state indices of both aragonite and calcite were <1 in the upper PRE (upstream of Humen Outlet, salinity <15), suggesting under-saturation for both aragonite and calcite minerals. In the area downstream of the Humen Outlet, Ω_{Ca} increased to ∼5.2 in 2005 and 4.0 in 2019, and Ω_{Ar} increased to 3.2 in 2005 and 2.4 in 2019, at the seawater end-member (**Figure 6**). The higher saturation state indices of calcite and aragonite in the high salinity zone in 2005 were due mainly to a local phytoplankton bloom, which was consistent with the relatively higher pH and DO, but lower DIC, in 2005.

Bulk Oxygen Consumption and Nitrification Rates

Bulk Oxygen Consumption Rate

In January of 2005 and 2019, DO decreased almost linearly during incubations without $HgCl_2$ addition, while DO concentrations remained almost constant for the samples with $HgCl_2$ added (control samples, **Figure 7**). The bulk oxygen consumption rates were 55.88 and 49.44 μmol L^{-1} d^{-1} in 2005 and 2019, respectively (**Table 1**).

In addition, we may use *in situ* DO concentrations to estimate the bulk oxygen consumption rate. In January 2005, DO saturation at the upstream-most station was 311.6 μmol kg^{-1}, while the *in situ* DO concentration was 14.9 μmol kg^{-1}. Therefore, the DO consumption was 296.7 μmol kg^{-1}. Assuming a residence time of 5 days (Guo et al., 2008), the DO consumption rate would be 59.3 μmol L^{-1} d^{-1}. This value is consistent with the value of 55.9 μmol L^{-1} d^{-1} estimated based on the incubations (**Table 1**). In January 2019, the *in situ* DO concentration at Guangzhou was 45.6 μmol kg^{-1} and the DO saturation was 302.7 μmol kg^{-1}. Therefore, the *in situ* DO consumption was 257.1 μmol kg^{-1}. If a residence time of 5 days is adopted (Guo et al., 2008), the bulk oxygen consumption rate is estimated as 51.4 μmol L^{-1} d^{-1}, which is reasonably consistent with values based on the incubations (49.4 μmol L^{-1} d^{-1}, **Table 1**).

Compared to other estuaries, the bulk oxygen consumption rate measured in the upper PRE is similar to that estimated in the polluted Seine River estuary in the spring and fall of 1996 [20–68 μmol L^{-1} d^{-1} assuming an average depth of 5 m, Garnier et al. (2001)]. However, it is higher than that found in the inner Scheldt estuary in the winter of 2003 [18–21 μmol L^{-1} d^{-1}, Gazeau et al. (2005)], or the polluted Huangpu River flowing through the city Shanghai (a branch of the lower Changjiang) in the winter and fall of 2005, which was 4–11 μmol L^{-1} d^{-1} (Zhai et al., 2007). However, it is lower than in salt marsh waters of the southeastern United States measured during the fall of 1995 and summer of 1996 [80 μmol L^{-1} d^{-1}, Cai et al. (1999)].

Nitrification Rate

In January 2005 and 2019, NO_2^- concentrations decreased in the samples with ATU added (inhibiting the oxidation of NH_4^+ to NO_2^-) during the incubations, suggesting the conversion of NO_2^- to NO_3^-. However, the NO_2^- concentration increased in the incubations with $NaNO_3$ added (inhibiting the oxidation

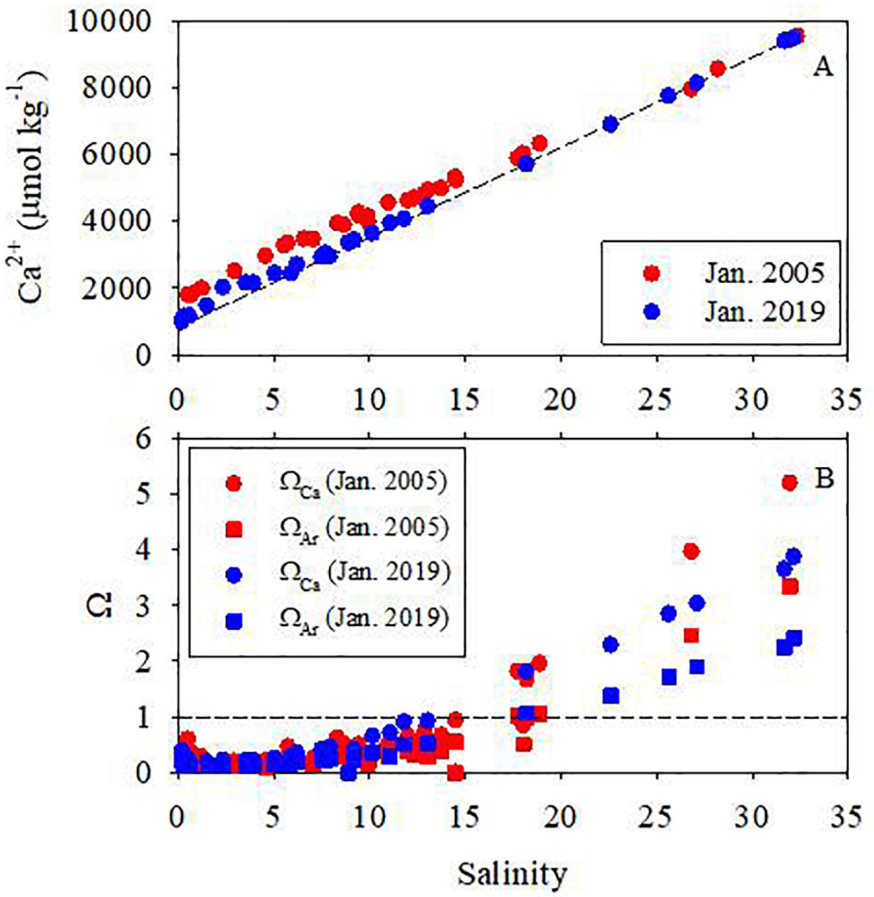

FIGURE 6 | Distributions of Ca^{2+} concentration and saturation state indices of calcite (Ω_{Ca}) and aragonite (Ω_{Ar}) in the surface water of the Pearl River estuary. The dashed line in panel **(A)** is the conservative mixing line. The dashed line in panel **(B)** represents $\Omega = 1$. Legends are the same for both panels.

of NO_2^- to NO_3^-), suggesting the accumulation of NO_2^- by converting NH_4^+ to NO_2^- (**Figure 8**). The estimated NH_4^+ oxidation rate was 3.86 μmol L^{-1} d^{-1} in 2005 and 6.53 μmol L^{-1} d^{-1} in 2019. The NO_2^- oxidation rate was 4.62 μmol L^{-1} d^{-1} in 2005 and 7.75 μmol L^{-1} d^{-1} in 2019 (**Table 1**). Nitrification rates in January of 2019 were higher than in January of 2005, but lower than in spring and summer [up to 31.5 μmol L^{-1} d^{-1}, Dai et al. (2008)]. Although NH_4^+ concentrations were lower in 2019 compared to 2005, the nitrification rate increased, which suggests that NH_4^+ concentrations are controlled by multiple factors. As the influencing factors of nitrification are beyond the scope of this study, we will not discuss it further here.

DISCUSSION

Processes Dominating DIC and TA Addition/Removal in the Upper PRE

Compared to January 2005, DIC and TA concentrations at the upstream-most station in January 2019 were both ∼1000 μmol kg^{-1} lower, but relatively consistent in the seawater end-member between both years. Influenced by the water characterized by very high DIC and TA at the upstream-most station, DIC and TA in the estuarine mixing zone at salinities <20 in January 2019 were much lower than those in January 2005 (**Figure 5**). It should be noted that DIC was slightly lower and pH and DO were slightly higher at the seawater end-member in 2005 (**Figures 5A-1,C-1,D-1**), which might be due to a weak local phytoplankton bloom.

The DIC and TA minima at salinity of ∼5 in 2019 were observed where the East River converges into the main channel of the estuary. Therefore, they might be due to the influence of East River water which was characterized by lower DIC and TA (the blue triangles in **Figures 5A-1,B-1**). DIC and TA in the East River were 605.3 and 566.6 μmol kg^{-1} in February 2019. The characteristically low DIC and TA concentrations of East River water were also reported in Guo et al. (2008). However, DIC and TA did not show this minima in January 2005, which might be due to large DIC and TA additions from local biogeochemical processes, similar to the case in the Guangzhou region.

Although both DIC and TA decreased downstream from the Guangzhou region, the very high DIC and TA values at the upstream-most station (3329.2 and 3093.5 μmol kg^{-1} in January 2005 and 2301.3 and 1947.2 μmol kg^{-1} in January

TABLE 1 | Environmental factors, air-water CO_2 flux (FCO_2), bulk oxygen consumption and nitrification rates of the water of the incubation station in the upper Pearl River estuary.

Time	Temp. (°C)	Salinity	NH_4^+ (μmol kg^{-1})	NO_2^- (μmol kg^{-1})	NO_3^- (μmol kg^{-1})	DO (μmol kg^{-1})	FCO_2 (mmol m^{-2} d^{-1})	O_2 consumption rate (μmol O_2 L^{-1} d^{-1})	NH_4^+ oxidation rate (μmol N L^{-1} d^{-1})	NO_2^- oxidation rate (μmol N L^{-1} d^{-1})
January 2005	16.0	0.69	838.2	68.3	107.9	15.4	175.5 ± 14.5	55.88	3.86	4.62
January 2019	16.4	0.31	155.2	43.2	424.3	45.7	174.5 ± 1.5	49.44	6.53	7.75

Nutrient data and nitrification rates for January 2005 are from Dai et al. (2008).

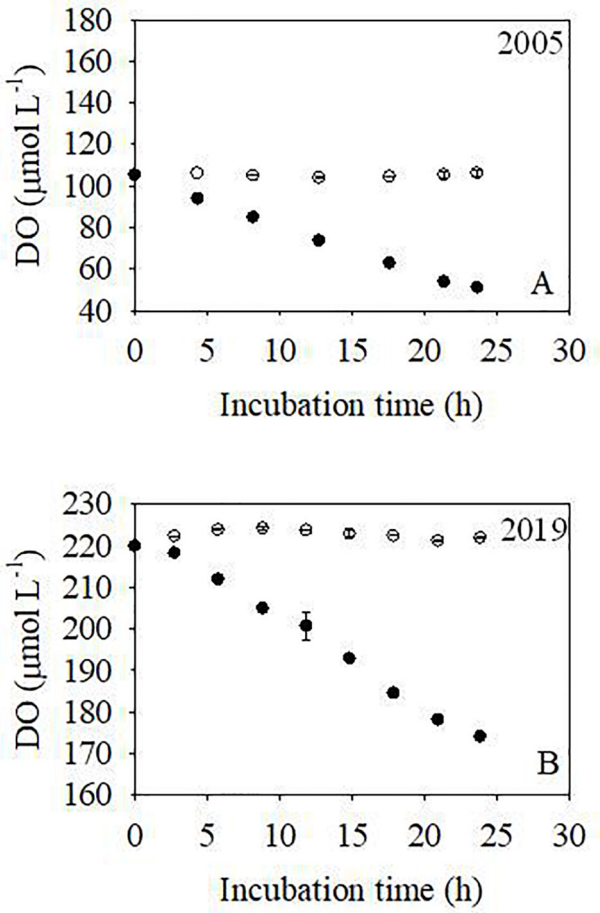

FIGURE 7 | Evolution of DO concentration during the incubations at the upstream-most station (Guangzhou). The solid circles are the samples without $HgCl_2$ addition; the open circles are the controls (samples with $HgCl_2$ added). Legends are the same for both panels.

2019, respectively) were not the river end-member values. The freshwater in the Guangzhou region was mostly from a branch of the North River. DIC and TA in the North River were 1587.5 and 1533.5 μmol kg^{-1} in January 2005 and 1575.4 and 1516.6 μmol kg^{-1} in January 2019 (Guo et al., unpublished data). DIC and TA in the East River were much lower. Therefore, there were local DIC and TA additions (1735.6 and 1549.2 μmol kg^{-1} additions in January 2005 and 707.4 and 539.5 μmol kg^{-1} additions in January 2019) in the Guangzhou region of the upper PRE.

Biogeochemical processes in the Guangzhou region of the upper PRE were very strong (Dai et al., 2006, 2008). Processes influencing DIC and TA concentrations include aerobic respiration, nitrification, air-water exchange of CO_2, and others (Guo et al., 2008). Benthic release is also an important DIC and TA source for the water column (Cai et al., 2015). Additionally, calcium carbonate dissolution or precipitation might also impact the carbonate system in estuarine environments (Abril et al., 2004; Macreadie et al., 2017; Su et al., 2020).

This complicated mixing scheme in the upper PRE makes it difficult to quantify the DIC and TA budget at all stations; thus, we take the upstream-most station as an example to quantify the influences of biogeochemical processes. At this station, the freshwater source was mainly the North River.

Air-Water CO_2 Exchange

The upper PRE was a strong CO_2 source. CO_2 evasion decreases DIC in the water, but has no influence on TA. The average air-water CO_2 exchange rate in the Guangzhou region was 175.5 ± 14.5 and 174.5 ± 1.5 mmol m^{-2} d^{-1} in January of 2005 and 2019, respectively (**Table 1**). If a residence time of 5 days and average water depth of 5 m are adopted (Zhao, 1990; Guo et al., 2008), the influence of CO_2 evasion would have decreased DIC by 175.5 and 174.5 μmol kg^{-1} in January 2005 and 2019, respectively. This shows the influence of CO_2 evasion on DIC was nearly identical in 2019 and 2005.

Pelagic Nitrification

The stoichiometric relationships of NH_4^+ and NO_2^- to DO and H^+ are expressed in Eqs. 5 and 6 (Dai et al., 2006). Only the oxidation of NH_4^+ to NO_2^- influences TA, and the ratio of change in TA to NH_4^+ concentrations is 2. Nitrification decreases TA in the water, but has no influence on DIC. At the upstream-most station, NH_4^+ oxidation rates were 3.86 μmol L^{-1} d^{-1} in January 2005 and 6.53 μmol L^{-1} d^{-1} in January 2019 (**Table 1**). Therefore, the rates of change in TA were 7.7 and 13.1 μmol L^{-1} d^{-1} in 2005 and 2019, respectively. Similarly, taking a residence time of 5 days (Guo et al., 2008), the TA change would be −38.6 and −65.3 μmol L^{-1} in 2005 and 2019.

$$NH_4^+ + 3/2O_2 \rightarrow NO_2^- + 2H^+ + H_2O \quad (5)$$

$$NO_2^- + 1/2\,O_2 \rightarrow NO_3^- \quad (6)$$

Organic Carbon Oxidation

The total oxygen consumption rate includes the oxygen consumption due to nitrification and organic carbon oxidation. During nitrification, the stoichiometric ratio of O_2 to NH_4^+ is 1.5 during the NH_4^+ oxidation process, and the ratio of O_2 to NO_2^- is 0.5 during the NO_2^- oxidation process (Eqs. 5 and 6). The NH_4^+ oxidation rate was 3.86 μmol L^{-1} d^{-1} in 2005 and 6.53 μmol L^{-1} d^{-1} in 2019, and the NO_2^- oxidation rate was 4.62 μmol L^{-1} d^{-1} in 2005 and 7.75 μmol L^{-1} d^{-1} in 2019 (**Table 1**). Therefore, the oxygen consumption rate induced by nitrification was 8.10 μmol O_2 L^{-1} d^{-1} in January 2005 and 13.69 μmol O_2 L^{-1} d^{-1} in January 2019, respectively.

As the total oxygen consumption rate at this station was 55.88 μmol L^{-1} O_2 d^{-1} in January 2005 and 49.44 μmol L^{-1} O_2 d^{-1} in January 2019, the DO consumption rate induced by the oxidation of organic carbon (excluding oxidation of nitrogen) was 47.78 μmol L^{-1} O_2 d^{-1} in January 2005 and 35.75 μmol L^{-1} O_2 d^{-1} in January 2019. According to the stoichiometric ratio of organic carbon oxidation (excluding nitrification of NH_4^+, Eq. 7), the DIC production rate due to organic carbon oxidation would be 47.78 μmol C L^{-1} d^{-1} in January 2005 and 35.75 μmol C L^{-1} d^{-1} in January 2019. If a residence time of 5 days is assumed (Guo et al., 2008), the DIC addition due to organic carbon oxidation would have been 238.9 μmol kg^{-1} in January 2005 and 178.8 μmol kg^{-1} in January 2019.

$$(CH_2O)_{106} + 106\,O_2 \rightarrow 106\,CO_2 + 106\,H_2O \quad (7)$$

$CaCO_3$ Dissolution

As the saturation state of $CaCO_3$ in the upper PRE ($\Omega < 0.5$) was well below the saturation level ($\Omega = 1$), $CaCO_3$ should dissolve. $CaCO_3$ dissolution influences both DIC and TA. We estimated the Ca^{2+} addition resulting from $CaCO_3$ dissolution according to the difference between the observed and estimated conservative mixing Ca^{2+} concentrations. To estimate the conservative Ca^{2+} concentration, we assume two end-member mixing between North River water and seawater. The relationship of the conservative mixing line of Ca^{2+} with salinity is expressed by Eq. 8.

$$[Ca^{2+}]\ (\mu mol\ kg^{-1}) = 278.75 \times \text{salinity} + 822.4 \quad (8)$$

In January 2005, the conservative Ca^{2+} concentration at the upstream-most station was 957.3 μmol kg^{-1}. As the measured Ca^{2+} concentration was 1691.8 μmol kg^{-1}, the Ca^{2+} addition was 734.4 μmol kg^{-1}. Since $CaCO_3$ dissolution adds DIC and TA by 1 and 2 times the amount of $CaCO_3$ dissolved (Eq. 9), the DIC and TA additions resulting from $CaCO_3$ dissolution were 734.4 and 1468.8 μmol kg^{-1}, respectively. Similarly, the conservative and observed Ca^{2+} concentrations were 882.9 and 1051.8 μmol kg^{-1} in January 2019, and the Ca^{2+} addition was 168.9 μmol kg^{-1}. The DIC and TA additions resulting from $CaCO_3$ dissolution were 168.9 and 337.8 μmol kg^{-1}, respectively. These estimates show that $CaCO_3$ dissolution in 2019 was much weaker than in 2005.

$$CaCO_3 + H^+ \leftrightarrow Ca^{2+} + HCO_3^- \quad (9)$$

The relatively lower $CaCO_3$ dissolution in January 2019 might be due to the relatively higher pH (**Figures 5C-1,C-2**). Low pH is favorable for $CaCO_3$ dissolution. Therefore, the relatively lower pH in 2005 might enhance $CaCO_3$ dissolution. However, $CaCO_3$ dissolution increases pH (Eq. 9), which adds the complexity of the relationship between pH and $CaCO_3$ dissolution.

Benthic Release

Denitrification can also influence DIC and TA (Chen, 2002), but as the water column was generally oxygenated (although DO < 60 μmol kg^{-1}) we assumed denitrification was negligible. However, both nitrification and denitrification might occur in the sediments of the PRE, which also influences the carbonate system in the water (Xu et al., 2005). Other anaerobic reactions (reduction of Fe/Mn and/or sulfate) in the sediment might also affect the carbonate system in the water. Anaerobic reactions in sediment consume protons and increase TA in the sediment porewater. Combined with the organic carbon degradation, DIC in porewater in the PRE was much higher than in the water column (Cai et al., 2015). The interactions between sediment and water at the water-sediment interface cause the sediment to release DIC and TA to the water column. A similar phenomenon of sedimentary reactions altering the

carbonate system in the water column was also observed in the northern Gulf of Mexico (Hu et al., 2017; Berelson et al., 2019).

As we didn't measure benthic fluxes during the cruises, we used the benthic DIC flux measured in November 2013 and the benthic TA/DIC ratio reported in the literature to estimate the influence of benthic release on the water column DIC and TA. In November 2013, the benthic DIC release rate at the upstream station was 1200 ± 300 mmol m^2 d^{-1} (Cai et al., 2015).

To account for the large influence of temperature on the rates of biogeochemical processes (Rabus et al., 2002; Govorushko, 2012), we calibrated the biogeochemical process rates in the sediment according to Eq. 10.

$$Q_{10} = e^{10k} \quad (10)$$

Q_{10} refers to the multiple of the increase in the rate of biochemical reactions per temperature increase of 10°C; k refers to the slope of the linear regression between temperature and the logarithm of rates.

The reported Q_{10} of anaerobic reactions in sediment ranges from 2 to 3 (Pomeroy and Wiebe, 2001; Kirchman et al., 2009), so a Q_{10} of 2.5 was taken in the estimation. The temperature in November 2013 when the sampling of Cai et al. (2015) was conducted was 22°C, while temperatures during our January 2005 and 2019 samplings were 16.0 and 16.4°C. Lowering the temperature by 6 and 5.6°C decreases the reaction rates by 1.73 and 1.67, respectively. Assuming that other conditions during our cruises were the same as November 2013, the benthic DIC release rate was 692.5 μmol m^2 d^{-1} in January 2005 and 718.3 μmol m^2 d^{-1} in January 2019.

The ratio of the benthic TA/DIC flux is 0.57–0.95 in the hypoxic northern Gulf of Mexico (Berelson et al., 2019). If this ratio range is similar in the PRE, the benthic TA flux would be 394.7–657.9 mmol m^{-2} d^{-1} in January 2005 and 409.5–682.4 mmol m^{-2} d^{-1} in January 2019.

The Guangzhou region of the upper PRE was well-mixed vertically, so the released benthic DIC and TA were likely homogenized throughout the whole water column. Taking an average water depth of 5 m and a residence time of 5 days (Zhao, 1990; Guo et al., 2008), the DIC and TA additions from the benthic flux would be 695.2 and 394.7–657.9 μmol kg^{-1} in January 2005, and 718.3 and 409.5–682.4 μmol kg^{-1} in January 2019. Therefore, considering the uncertainties in the benthic DIC and TA flux estimates, no conspicuous changes were observed between January 2005 and January 2019.

Inter-annual Variations in DIC and TA in the Upper PRE

The quantification of the above biogeochemical processes at the upstream-most station is shown in **Table 2**. The net influence of these biogeochemical processes was 1490.3 and 1824.9–2088.1 μmol kg^{-1} for DIC and TA in January 2005, and 895.1 and 682.0–954.9 μmol kg^{-1} for DIC and TA in January 2019. The estimates were generally consistent with the observed DIC and TA additions (1735.6 and 1549.2 μmol kg^{-1} in January 2005, and 707.4 and 539.5 μmol kg^{-1} in January 2019) at this station.

TABLE 2 | Quantified influences of biogeochemical processes on DIC and TA (ΔDIC and ΔTA) at Guangzhou in January of 2005 and 2019.

Biogeochemical processes	ΔDIC (μmol kg^{-1})		ΔTA (μmol kg^{-1})	
	2005	2019	2005	2019
CO_2 evasion	−175.5	−174.5	0.0	0.0
Pelagic nitrification	0.0	0.0	−38.6	−65.3
Organic carbon oxidation	238.9	178.8	0.0	0.0
$CaCO_3$ dissolution	734.4	168.9	1468.8	337.8
Benthic release	692.5	718.3	394.7–657.9	409.5–682.4
Net impact	1490.3	891.5	1824.9–2088.1	682.0–954.9
Observed addition	1735.6	707.4	1549.2	539.5

The only DIC sink for upper PRE water in January of both 2005 and 2019 was CO_2 evasion to the atmosphere, while the DIC sources were organic carbon oxidation, $CaCO_3$ dissolution and benthic release. The DIC removal due to CO_2 evasion to the atmosphere was almost the same during the two winter cruises (175.5 and 174.5 μmol kg^{-1} in 2005 and 2019, respectively). Although the DIC addition from organic carbon oxidation in January 2019 was slightly lower than in January 2005 (238.9 μmol kg^{-1} in 2005 vs. 178.8 μmol kg^{-1} in 2019), DIC removal due to CO_2 evasion was almost offset by the DIC addition resulting from organic carbon oxidation during both cruises relative to the size of the overall DIC budget. The most important sources of DIC were $CaCO_3$ dissolution and benthic release. As the benthic release rates were estimated based on previously reported benthic DIC fluxes and only the temperature effect was considered, estimates of benthic DIC release were similar during the two winter cruises as the temperatures were similar. A comparison between the two winter cruises indicates the largest differences were in the DIC addition due to $CaCO_3$ dissolution; DIC addition due to this process was 565.5 μmol kg^{-1} lower in January 2019 than in January 2005, controlling the much lower overall DIC addition observed in January 2019.

The only major sink for TA of the water was pelagic nitrification. As the nitrification rate in January 2019 was slightly higher than in January 2005, the TA removal in 2019 (65.3 μmol kg^{-1}) was slightly greater than in 2005 (38.6 μmol kg^{-1}). As was the case with DIC, the benthic TA release during both the 2005 and 2019 cruises was similar. However, the TA addition due to $CaCO_3$ dissolution in January 2019 was 1131.0 μmol kg^{-1} lower than in 2005, and dominated the decrease in the local TA addition in 2019 in the upper PRE.

Although the above estimates generally explain the inter-annual variations in DIC and TA in the upper PRE between 2005 and 2019, there are differences between the sum of the estimated and the observed addition values. These differences might be due to the different dynamic conditions during the different cruises as well as the uncertainties in estimating benthic DIC and/or TA fluxes. The uncertainties in water residence time, average depth, and other parameters might also add to the uncertainties of the estimates. In addition, the influence of complicated mixing on the biogeochemical processes across the entire estuarine mixing

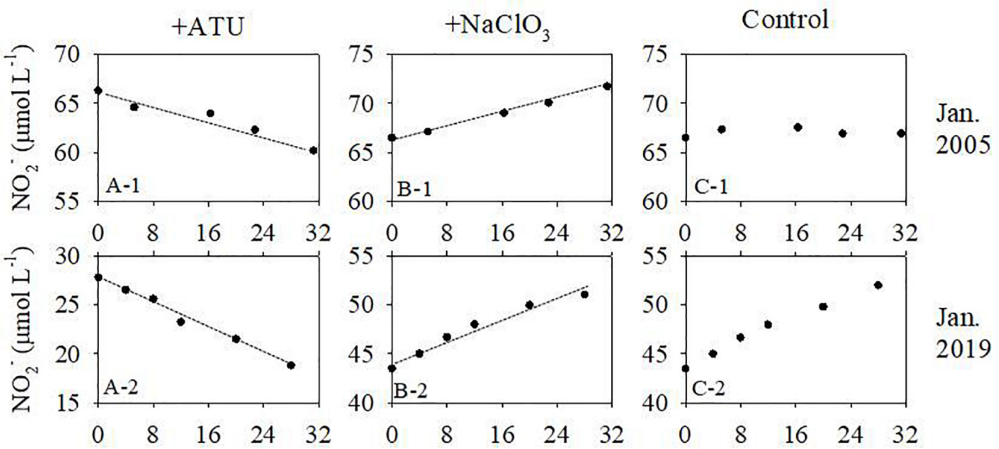

FIGURE 8 | Evolution of NO_2^- concentration during the nitrification incubations. The dashed lines are linear regressions. Data for January 2005 are from Dai et al. (2008). Labels are the same for all panels.

zone is yet to be quantified. The relationship between decreasing $CaCO_3$ dissolution and the improvement of water quality also needs further examination.

Ecological environmental improvement is a universal goal in China and across the world, and this may in turn influence the cycles of biogenic elements. Similar inter-annual variability in biogeochemical parameters or mass fluxes may manifest in other estuaries and coastal zones, which could also influence ocean element cycling and even local climate change. This phenomenon deserves more attention.

CONCLUSION

Dissolved inorganic carbon and TA distributions in the PRE were determined in January of 2005 and 2019. Although they show little difference in the high-salinity lower estuary, both DIC and TA in the heavily perturbed upper estuary showed a ∼1000 μmol kg^{-1} decrease in 2019 compared to 2005. The upstream-most station was used as an example to quantify the influences of biogeochemical processes on DIC and TA. For DIC, the CO_2 degassing was almost compensated by organic carbon oxidation, while benthic release and $CaCO_3$ dissolution contributed to the major additions. For TA, benthic release and $CaCO_3$ dissolution were the major additions, and pelagic nitrification contributed to slight removal. Although the above biogeochemical processes differed between the 2 years, the decrease in $CaCO_3$ dissolution dominated the DIC and TA decreases in the upper PRE in 2019 compared to 2005. In the context of global change, inter-annual variability in the biogeochemical parameters of estuaries and coasts might be universal and deserves more attention.

DATA AVAILABILITY STATEMENT

The raw data supporting the conclusions of this article will be made available by the authors, without undue reservation.

AUTHOR CONTRIBUTIONS

XG collected the oxygen consumption rate data from the January 2005 cruise. All authors collected the data from the January 2019 cruise except LW. XG designed the cruise, took the DIC, TA and pH samples. XS and YG conducted the nitrification and oxygen consumption incubation experiments. YL collected the nutrient and calcium samples. YX measured DO and pCO_2. TH measured the ammonium samples. YG and YL measured the N + N, phosphate and silicate samples. XS and YL measured the DIC, TA and calcium samples. YG and YL collected the North and East Rivers data in February 2019. XG drafted the manuscript and all authors participated the discussion on data interpretation.

FUNDING

This study was supported by the National Natural Science Foundation of China (grant numbers 41876080 and 41706079). The preparation of this manuscript was supported by the Strategic Priority Research Program of Chinese Academy of Sciences (grant number XDB42000000) and Hong Kong Research Grants Council (grant number T21-602/16-R).

ACKNOWLEDGMENTS

We are grateful to the crews of the ships Yue-Dong-Guan-Yu 00589 and Yue-Zhu-Yu 31008 for their help during the cruises. Baoshan Chen is appreciated for collecting the calcium data during the January 2005 cruise. Weifang Chen, Wen Lin, Yan Li, and Zhe Wang at Xiamen University, Dr. Huabin Mao at the South China Sea Institute of Oceanography (Chinese Academy of Sciences) and Ms. Haijuan Chen at Xinzhou Hotel (Guangzhou) are appreciated for their help in preparation and implementation of the cruises. The discussion with Dr. Wei-Jun Cai at University of Delaware was helpful in data interpretation.

REFERENCES

Abril, G., Commarieu, M. V., Maro, D., Fontugne, M., Guerin, F., and Etcheber, H. (2004). A massive dissolved inorganic carbon release at spring tide in a highly turbid estuary. *Geophys. Res. Lett.* 31:L09316.

Bendtsen, J., and Hansen, J. L. S. (2013). Effects of global warming on hypoxia in the Baltic Sea-North Sea transition zone. *Ecol. Model.* 264, 17–26. doi: 10.1016/j.ecolmodel.2012.06.018

Benson, B. B., and Krause, D. (1984). The concentration and isotopic fractionation of oxygen dissolved in freshwater and seawater in equilibrium with the atmosphere. *Limnol. Oceanogr.* 29, 620–632. doi: 10.4319/lo.1984.29.3.0620

Berelson, W. M., McManus, J., Severmann, S., and Rollins, N. (2019). Benthic fluxes from hypoxia-influenced Gulf of Mexico sediments: impact on bottom water acidification. *Mar. Chem.* 209, 94–106. doi: 10.1016/j.marchem.2019.01.004

Caballero-Alfonso, A. M., Carstensen, J., and Conley, D. J. (2015). Biogeochemical and environmental drivers of coastal hypoxia. *J. Mar. Syst.* 141, 190–199. doi: 10.1016/j.jmarsys.2014.04.008

Cai, P., Shi, X., Hong, Q., Li, Q., Liu, L., Guo, X., et al. (2015). Using 224Ra/228Th disequilibrium to quantify benthic fluxes of dissolved inorganic carbon and nutrients into the Pearl River Estuary. *Geochim. Cosmochim. Acta* 170, 188–203. doi: 10.1016/j.gca.2015.08.015

Cai, W.-J., Dai, M. H., Wang, Y. C., Zhai, W. D., Huang, T., Chen, S. T., et al. (2004). The biogeochemistry of inorganic carbon and nutrients in the Pearl River estuary and the adjacent Northern South China Sea. *Continent. Shelf Res.* 24, 1301–1319. doi: 10.1016/j.csr.2004.04.005

Cai, W.-J., Pomeroy, L. R., Moran, M. A., and Wang, Y. C. (1999). Oxygen and carbon dioxide mass balance for the estuarine-intertidal marsh complex of five rivers in the southeastern U S. *Limnol. Oceanogr.* 44, 639–649. doi: 10.4319/lo.1999.44.3.0639

Cao, Z., and Dai, M. (2011). Shallow-water CaCO3 dissolution: evidence from excess calcium in the South China Sea and its export to the Pacific Ocean. *Glob. Biogeochem. Cycles* 25:GB2019.

Carpenter, J. H. (1965). The chesapeake Bay Institute technique for the Winkler dissolved oxygen method. *Limnol. Oceanogr.* 10, 141–143. doi: 10.4319/lo.1965.10.1.0141

Carstensen, J., Andersen, J. H., Gustafsson, B. G., and Conley, D. J. (2014). Deoxygenation of the Baltic Sea during the last century. *Proc. Natl. Acad. Sci. U.S.A.* 111, 5628–5633. doi: 10.1073/pnas.1323156111

Chen, C.-T. A. (2002). Shelf vs. dissolution-generated alkalinity above the chemical lysocline. *Deep Sea Res. II* 49, 5365–5375. doi: 10.1016/s0967-0645(02)00196-0

Chen, J., and He, D. (1999). Chemical characteristics and genesis of major ions in the Pearl River basin. *Acta Sci. Nat. Univ. Pekinesis* 35, 786–793.

China-EPA (1987). Water quality-determination of calcium-EDTA titrametric method. National standards of people's republic of China. *Natl. Environ. Protect. Agency Peoples Republic China* 87, 56–59.

Conley, D. J., Carstensen, J., Aigars, J., Axe, P., Bonsdorff, E., Eremina, T., et al. (2011). Hypoxia is increasing in the Coastal Zone of the Baltic Sea. *Environ. Sci. Technol.* 45, 6777–6783.

Cui, Y., Wu, J., Ren, J., and Xu, J. (2019). Physical dynamics structures and oxygen budget of summer hypoxia in the Pearl River Estuary. *Limnol. Oceanogr.* 64, 131–148. doi: 10.1002/lno.11025

Dai, M., Gan, J., Han, A., Kung, H. S., and Yin, Z. (2014). *Physical Dynamics and Biogeochemistry of the Pearl River Plume, Biogeochemical Dynamics at Major River-Coastal Interface-Linkage with Global Change*. New York: Cambridge University Press, 321–352.

Dai, M., Wang, L., Guo, X., Zhai, W., Li, Q., He, B., et al. (2008). Nitrification and inorganic nitrogen distribution in a large perturbed river/estuarine system: the Pearl River Estuary, China. *Biogeosciences* 5, 1227–1244. doi: 10.5194/bg-5-1227-2008

Dai, M. H., Guo, X. H., Zhai, W. D., Yuan, L. Y., Wang, B. W., Wang, L. F., et al. (2006). Oxygen depletion in the upper reach of the Pearl River estuary during a winter drought. *Mar. Chem.* 102, 159–169. doi: 10.1016/j.marchem.2005.09.020

Dickson, A. G. (1990). Thermodynamics of the dissociation of boric acid in synthetic sea water from 273.15 to 318.15 K Deep. *Sea Res. A Oceanogr. Res. Pap.* 37, 755–766. doi: 10.1016/0198-0149(90)90004-f

EPA (1993). *Manual Nitrogen Control*. Washington DC: Office of Research and Development, Office of Water, United States Environmental Protection Agency.

Fennel, K., and Testa, J. M. (2019). Biogeochemical controls on coastal hypoxia. *Annu. Rev. Mar. Sci.* 11, 105–130. doi: 10.1146/annurev-marine-010318-095138

Garnier, J., Servais, P., Billen, G., Akopian, M., and Brion, N. (2001). Lower Seine River and estuary (France) carbon and oxygen budgets during low flow. *Estuaries* 24, 964–976. doi: 10.2307/1353010

Gazeau, F., Gattuso, J. P., Middelburg, J. J., Brion, N., Schiettecatte, L. S., Frankignoulle, M., et al. (2005). Planktonic and whole system metabolism in a nutrient-rich estuary (the Scheldt estuary). *Estuaries* 28, 868–883. doi: 10.1007/bf02696016

Govorushko, S. M. (2012). Influence of weather-climatic conditions on biospheric processes. *Atmos. Ocean. Phys.* 48, 771–784. doi: 10.1134/s0001433812080051

Guo, X. H., Cai, W.-J., Zhai, W. D., Dai, M. H., Wang, Y. C., and Chen, B. S. (2008). Seasonal variations in the inorganic carbon system in the Pearl River (Zhujiang) estuary. *Continent. Shelf Res.* 28, 1424–1434. doi: 10.1016/j.csr.2007.07.011

Guo, X. H., Dai, M. H., Zhai, W. D., Cai, W. J., and Chen, B. S. (2009). CO2 flux and seasonal variability in a large subtropical estuarine system, the Pearl River Estuary, China. *J. Geophys. Res. Biogeosci.* 114:G03013.

Han, A., Dai, M., Kao, S.-J., Gan, J., Li, Q., Wang, L., et al. (2012). Nutrient dynamics and biological consumption in a large continental shelf system under the influence of both a river plume and costal upwelling. *Limnol. Oceanogr.* 57, 486–502. doi: 10.4319/lo.2012.57.2.0486

Hansen, H. P., and Koroleff, F. (1999). *Determination of Nutrients, Methods of Seawater Analysis*. Toronto: Wiley-VCH, 159–228.

Hu, X., Li, Q., Huang, W.-J., Chen, B., Cai, W.-J., Rabalais, N. N., et al. (2017). Effects of eutrophication and benthic respiration on water column carbonate chemistry in a traditional hypoxic zone in the Northern Gulf of Mexico. *Mar. Chem.* 194, 33–42. doi: 10.1016/j.marchem.2017.04.004

Ingle, S. E. (1975). Solubility of calcite in the ocean. *Mar. Chem.* 3, 301–319. doi: 10.1016/0304-4203(75)90010-9

Kanamori, S., and Ikegami, H. (1980). Computer-processes potentiometric titration for the determination of calcium and magnesium in seawater. *J. Oceanogr. Soc. Jpn.* 36, 177–184.

Kirchman, D. L., Morán, X. A., and Ducklow, H. (2009). Microbial growth in the polar oceans—role of temperature and potential impact of climate change. *Nat. Rev. Microbiol.* 7, 451–459. doi: 10.1038/nrmicro2115

Lebel, J., and Poisson, A. (1976). Potentiometric determination of calcium and magnesium in seawater. *Mar. Chem.* 4, 321–332. doi: 10.1016/0304-4203(76)90018-9

Li, D. J., Zhang, J., Huang, D. J., Wu, Y., and Liang, J. (2002). Oxygen depletion off the Changjiang (Yangtze River) estuary. *Sci. China Ser. D Earth Sci.* 45, 1137–1146. doi: 10.1360/02yd9110

Li, M., Lee, Y. J., Testa, J. M., Li, Y., Ni, W., Kemp, W. M., et al. (2016). What drives interannual variability of hypoxia in Chesapeake Bay: climate forcing versus nutrient loading? *Geophys. Res. Lett.* 43, 2127–2134. doi: 10.1002/2015gl067334

Liang, B., Hu, J. T., Li, S. Y., Ye, Y. X., Liu, D. H., and Huang, J. (2020). Carbon system simulation in the Pearl River Estuary, China: mass fluxes and transformations. *J. Geophys. Res. Biogeosci.* 125:e2019JG005012.

Macreadie, P. I, Serrano, O., Maher, D. T., and Duarte, C. M. B. J. (2017). Addressing calcium crbonate cycling in blue carbon accounting. *Limnol. Oceanogr. Lett.* 2, 195–201. doi: 10.1002/lol2.10052

Millero, F. J. (1979). The thermodynamics of the carbonate system in seawater. *Geochim. Cosmochim. Acta* 43, 1651–1661. doi: 10.1016/0016-7037(79)90184-4

Millero, F. J. (2010). Carbonate constants for estuarine waters. *Mar. Freshw. Res.* 61, 139–142. doi: 10.1071/mf09254

Mucci, A. (1983). The solubility of calcite and aragonite in seawater at various salinities, temperatures, and one atmosphere total pressure. *Am. J. Sci.* 283, 780–799. doi: 10.2475/ajs.283.7.780

Olson, E. J., and Chen, C.-T. A. (1982). Interference in the determination of calcium in seawater. *Limnol. Oceanogr.* 27, 375–380. doi: 10.4319/lo.1982.27.2.0375

Pai, S. C., Tsau, Y.-J., and Yang, T.-I. (2001). pH and buffering capacity problems involved in the determination of ammonia in saline water using the indophenol blue spectrophotometric method. *Anal. Chim. Acta* 434, 209–216. doi: 10.1016/s0003-2670(01)00851-0

Pierrot, D., Lewis, E., and Wallace, W. R. (2006). *MS Excel Program Developed for CO2 System Calculations*. ORNL/CDIAC-105a. Oak Ridge: Carbon Dioxide Information Analysis Center.

Pomeroy, L. R., and Wiebe, W. J. (2001). Temperature and substrates as interactive limiting factors for marine heterotrophic bacteria. *Aquat. Microb. Ecol.* 23, 187–204. doi: 10.3354/ame023187

Qian, W., Gan, J., Liu, J., He, B., Lu, Z., Guo, X., et al. (2018). Current status of emerging hypoxia in a eutrophic estuary: the lower reach of the Pearl River Estuary, China. *Estua. Coast. Shelf Sci.* 205, 58–67. doi: 10.1016/j.ecss.2018.03.004

Rabalais, N. N., and Turner, R. E. (2006). *Oxygen Depletion in the Gulf of Mexico adjacent to the Mississippi River, Past and Present Water Column Anoxia*. Netherlands: Springer, 225–245.

Rabus, R., Bruchert, V., Amann, J., and Konneke, M. (2002). Physiological response to temperature changes of the marine,sulfate-reducing bacterium *Desulfobacterium autotrophicum*. *FEMS Microbiol. Ecol.* 42, 409–417. doi: 10.1111/j.1574-6941.2002.tb01030.x

Su, J., Cai, W.-J., Jean, B., Chen, B., Hussain, N., Yao, Y., et al. (2020). Chesapeake Bay acidification buffered by spatially decoupled carbonate mineral cyclin. *Nat. Geosci.* 13, 441–447. doi: 10.1038/s41561-020-0584-3

Sweeney, C., Gloor, E., Jacobson, A. R., Key, R. M., McKinley, G., Sarmiento, J. L., et al. (2007). Constraining global air-sea gas exchange for CO2 with recent bomb C-14 measurements. *Glob. Biogeochem. Cycles* 21: GB2015.

Testa, J. M., and Kemp, W. M. (2012). Hypoxia-induced shifts in nitrogen and phosphorus cycling in Chesapeake Bay. *Limnol. Oceanogr.* 57, 835–850. doi: 10.4319/lo.2012.57.3.0835

Wang, B., Hu, J., Li, S., Yu, L., and Huang, J. (2018). Impacts of anthropogenic inputs on hypoxia and oxygen dynamics in the Pearl River estuary. *Biogeosciences* 15, 6105–6125. doi: 10.5194/bg-15-6105-2018

Weiss, R. F. (1974). Carbon dioxide in water and seawater: the solubility of a non-ideal gas. *Mar. Chem.* 2, 203–215. doi: 10.1016/0304-4203(74)90015-2

Xu, J. R., Wang, Y. S., Wang, Q. J., and Yin, J. P. (2005). Nitrous oxide concentration and nitrification and denitrification in Zhujiang River estuary, China. *Acta Oceanol. Sin.* 24, 122–130.

Zhai, W. D., Dai, M. H., and Guo, X. H. (2007). Carbonate system and CO2 degassing fluxes in the inner estuary of Changjiang (Yangtze) River, China. *Mar. Chem.* 107, 342–356. doi: 10.1016/j.marchem.2007.02.011

Zhai, W. D., Zheng, N., Huo, C., Xu, Y., Zhao, H. D., Li, Y. W., et al. (2014). Subsurface pH and carbonate saturation state of aragonite on the Chinese side of the North Yellow Sea: seasonal variations and controls. *Biogeosciences* 11, 1103–1123. doi: 10.5194/bg-11-1103-2014

Zhao, H. (1990). *Evolution of the Pearl River Estuary*. Melbourne: Ocean Press.

Conflict of Interest: The authors declare that the research was conducted in the absence of any commercial or financial relationships that could be construed as a potential conflict of interest.